Nanoscale



PAPER

View Article Online
View Journal | View Issue



Cite this: Nanoscale, 2022, 14, 12030

Enhanced radioluminescence of yttrium pyrosilicate nanoparticles *via* rare earth multiplex doping

Eric Zhang,^{a,b} Yuriy Bandera,^{a,b} Ashley Dickey,^c Joseph W. Kolis^c and Stephen H. Foulger (1) *a,b,d

A series of multi-doped yttrium pyrosilicate (YPS) nanoparticles were synthesized using a high temperature multi-composite reactor, and used to explore the radioluminescent properties that have potential for biological applications. The luminescent activators explored in this work were cerium, terbium, and europium. A series of mono-doped YPS nanoparticles were synthesized that have optical and X-ray luminescent properties that span the entire visible spectrum. Energy transfer experiments were investiagted to increase the photo- and X-ray luminescence of terbium and europium. Cerium was used as a sensitizer for terbium where X-ray luminescence was enhanced. Similar results were also obtained using cerium as a sensitizer and terbium as an energy bridge for europium. By leveraging different energy transfer mechanisms X-ray luminescence can be enhanced for YPS nanoparticles.

Received 3rd May 2022, Accepted 25th July 2022 DOI: 10.1039/d2nr02417a

rsc.li/nanoscale

1 Introduction

In the past four decades, rare earth nanomaterials have been employed in many areas of biomedical research spanning diagnostics, imaging, and drug delivery. The chemistry of rare earth nanoparticles is well-established and researchers can engineer the size, shape, and composition of these particles for different biological requirements.2 These nanoparticles are commonly fluoride compounds that utilize upconversion processes where multiple low energy excitation wavelengths (i.e. infrared) are absorbed to generate higher energy emission.³ An alternative biomedical tool in its nascent stages is the use of radioluminescent nanoparticles coupled with deep tissue penetrating X-rays. In biomedical imaging, autofluorescence from cell medium, cell lysis, and hair hampers traditionally UV in vivo imaging techniques; however, optical X-ray luminescence technique can improve sensitivity. In theranostics, X-ray induced photodynamic therapy has gained popularity for its deep tissue penetration that traditionally cannot be reached by surgical or near infrared radiation.⁵ Other fields may benefit from deep penetrating and bright luminescence, such as optogenetics, where specific wavelengths of light can

Scintillators are a class of materials that can absorb high energy radiation such as X-rays and convert that energy into light.⁷ This is a notoriously inefficient process with nanoscintillators, as the excitation energy is lost through trapped states, energy migration from the medium (i.e. water) to the particle, and defects inherently generated at the nanoscale.8 Effective nanoscintillators with potential for biomedical applications must also have a high effective atomic number, high degree of crystallinity, be non-hydroscopic, and be non-toxic. 9,10 One potential candidate for X-ray active nanoparticles in the biomedical field is the family of lanthanide silicates. 11 A technique termed the "high temperature multi-composite reactor" (HTMcR) was developed to accommodate the synthesis of nanoscintillators that requires extreme temperatures (>1000°C) to create highly crystalline particulates while preventing aggregation of the nanoparticles. 12 This technique was used to synthesize yttrium pyrosilicate (Y₂Si₂O₇, YPS) and lutetium pyrosilicate (Lu₂Si₂O₇, LPS), both of which were doped with cerium, to generate a blue emission when exposed to X-ray radiation. Depending on the application, both YPS and LPS can host a multitude of other rare earth emitters that can exhibit emissions at different wavelengths.

control neural activities.⁶ In many biological applications like optogenetics, it is essential that that luminescent species be small enough to penetrate the various biological barriers typical in *in vivo* systems. Typically, this means that the materials must be approximately 100 nm or smaller as nonaggregated nanoparticles to be useful in biomedical applications.

^aDepartment of Materials Science and Engineering, Clemson University, Clemson, SC 29634-0971, USA. E-mail: foulger@clemson.edu

^bCenter for Optical Materials Science and Engineering Technologies (COMSET),

Anderson SC 29625 USA

^cDepartment of Chemistry, Clemson University, Clemson, SC 29634-0971, USA

^dDepartment of Bioengineering, Clemson University, Clemson, SC 29634-0971, USA

Nanoscale

The rare earth elements, apart from lanthanum and lutetium, have 4f electrons which have many electronic states that can generate unique luminescence spectra that span the entire visible spectrum. 13,14 The f-f transitions are characterized by sharp emissions, large Stokes shifts, and long lifetimes, all of which are ideal traits for biomedical applications. However these intra-4f transitions are forbidden by the Laporte rule so the absorption coefficients are very small (1-10 M⁻¹ cm⁻¹).¹⁵ Typically these rare earth elements are doped in a host lattice where a ligand (i.e. oxygen or other rare earth ions) is used to enhance absorption through an antenna effect. 16 An alternative method to control the optical output and luminescent color is to dope the crystal with multiple rare earths where a sensitizer can transfer its energy to the emitting ion. For example the strong broad band d-f emission of cerium is a well-known sensitizer to enhance the photoluminescence of terbium, 17 while color tuneability on the CIE diagram can be controlled by the ratio of two or more rare earths emitters. 18 By strategically choosing the right rare earth emitters during synthesis, a diverse range of photoluminescent emissions can begenerated. 13 In contrast, X-ray luminescence energy transfer between rare earth ions in nanocrystals is not as widely studied and therefore has many more opportunities for exploration.

In both imaging and therapeutics, a scintillator acts as a transducer that can convert the high energy radiation into visible light with a specific wavelength.19 In addition to high output intensity, a scintillator should have good spectral overlap with its respective biological conjugate. The emission wavelength must have a spectral overlap with its respective conjugate. This biological conjugate in imaging would be the detector, 20 for X-ray induced photodynamic therapy it is the photosensitizer,²¹ and for X-ray optogenetics it is the light sensitive protein.22 In this regard, inorganic scintillators are the ideal candidates for X-ray related biomedical applications because of the broad emission domain accessible with various dopants.23 Furthermore, the inherent high atomic number of inorganic materials have a high stopping power to efficiently absorb high energy photons.24

Due to the limitations of scintillator brightness in nanoparticles as described above, numerous studies have also been reported to increase the light yield of nanophosphors using creative multi-doping strategies.²⁵ When using these rare earth emitters in conjunction with the HTMcR process, high density and fully crystalline nanoparticles can be synthesized that have enhanced X-ray related properties for biomedical applications. In this report, a nano-YPS host lattice was used to investigate the X-ray luminescence energy transfer between cerium, terbium, and europium. This was accomplished through a series of mono-, co-, and tri-doped systems using the HTMcR where the mono-doped system served as a benchmark for the cerium/terbium co-doped system and the cerium/ terbium/europium tri-doped system. To the best of our knowledge, this is the first time radioluminescence energy transfer between cerium, terbium, and europium were explored in yttrium pyrosilicate nanoparticles synthesized via a high temperature multi-composite reactor.

Results and discussion

Yttrium pyrosilicate (Y₂Si₂O₇) exhibits six different structures depending on the temperature and doping/stabilizing agents used during synthesis.²⁶ When employing the HTMcR at 1100°C with a silica core and cerium doped yttrium shell, the particulates recrystallize into the triclinic crystal structure with a P1 space group. In this structure, the cerium dopant can substitute at either the distorted trigonal or octahedral site of Y³⁺, both of which are acentric, which increases the probability for the allowed electronic f-d transition to occur.²⁷ In this report, the active emitters are cerium, terbium, and europium ions with the same oxidation state as yttrium and will substitute at the same acentric sites. No polymorphs of the various doped YPS nanoparticles were observed during the crystallization process (Fig. 1) and all products crystallized in the triclinic phase. All mono-, co-, and tri-doped particulates were annealed at 1100°C for 18 hours with the highest doping concentration being the tri-doped system which was doped at 30.75 mol% of yttrium. Furthermore, the consistent crystal structure obtained at such a high concentration of cerium, terbium, and europium would suggest that the YPS particulates can be doped with other rare earth emitters and crystallize exclusively in the triclinic space group due to the similar size and oxidation state of the lanthanide series. 28 This has the potential to explore unique optical properties that can only be observed by f-f transition.

All nanoparticle sets were synthesized by the HTMcR process. This enabled us to prepare a variety of multidoped nanoparticles and convert them to the crystalline triclinic phase while maintaining the non-aggregated, well dispersed nature of the nanoparticles. Transmission electron microscopy (TEM) shows the well dispersed, cleanly doped nature of the

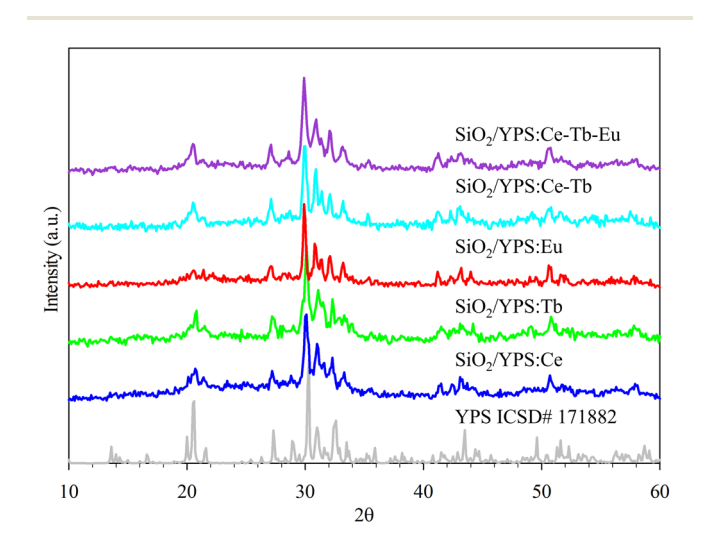


Fig. 1 X-ray diffraction of different YPS particulates mono-doped with cerium (0.75%), terbium (10%), europium (15%), co-doped with cerium (0.75%) and terbium (10%), and tri-doped with cerium (0.75%), terbium (15%), and europium (15%). All X-ray diffraction traces were compared to a single crystal YPS crystal ICSD #171882.

Paper Nanoscale

nanoparticles with the various mono-, bi- and tridoped silica core and yttrium pyrosilicate shell (Fig. 2a-e). The dispersed spherical nanoparticles would suggest that the HTMcR process does an excellent job in preventing irreversible aggregation at the elevated temperatures of the annealing conditions. The average particle size of YPS:Ce, YPS:Tb, YPS:Eu, YPS:Ce-Tb, and YPS:Ce-Tb-Eu are all between 140 nm-150 nm with no statistical difference between each set. The similar final particle size is expected in all other cases as well, since the same silica core was used throughout the different sets of particulates and is the size template for the core-shell particles. A core-shell formation can be observed from all the particulates by their EM contrast, where the dark contrast represents the heavier atomic elements composed of vttrium, cerium, terbium, and europium while, the lighter contrast represents the silica core. Interestingly, the YPS:Ce-Tb-Eu image presented has a particle with a partial shell (cf. Fig. 2e and i). Upon closer examination, the electron dispersive spectroscopy (EDS) images exhibit overlap of the rare earth elements with the dark contrast regions of the TEM images, supporting the postulate that core-shell structures were formed in the HTMcR process (Fig. 2f-h and j-l). The elemental mapping demonstrates that yttrium, cerium, terbium, and europium are uniformly distributed throughout the shell.

Fig. 3 shows the optical and X-ray luminescence of monodoped Ce³⁺, Tb³⁺, and Eu³⁺ in the YPS particulates. When doped with cerium, the optical and X-ray luminescence properties exhibit the same d-f transitions previously reported, where a slight red shift is observed due to the silica core's

X-ray luminescence. 12 Both the terbium and europium doped particulates were excited at their optimal excitation wavelength of 250 nm. Terbium doped YPS particulates exhibits four photoluminescence peaks at 493 nm, 542 nm, 590 nm, and 623 nm corresponding to the electron relaxation from 5D4 state to the ⁷F₆, ⁷F₅, ⁷F₄, and ⁷F₃ states respectively.²⁹ The mono-doped europium system has four peak regions at 580-600 nm, 610-620 nm, 650-660 nm, and 690-700 nm which are ascribed to the relaxation of electrons from the ⁵D₀ state to the ⁷F₁, ⁷F₂, ⁷F₃, ⁷F₄ states, respectively. ³⁰ Notably both terbium and europium doped systems have matching photoluminescence and X-ray luminescence while, the X-ray luminescence of cerium is somewhat red shifted. This can be attributed to the d-f transition in cerium, where the d-orbitals are influenced by the crystal lattice and the defects inherent to nanoparticles. The combination of these dopants can be strategically determined during synthesis to maximize the coupling of their X-ray luminescences with the potential biological conjugates such as opsins. In optogenetics, the chosen light sensitive proteins will only respond to specific wavelengths of photons. For example, channel rhodopsin-2 has the potential to absorb the emission from YPS:Ce while a red-activatable channel rhodopsin can absorb the emission of YPS:Eu due to the spectral overlap between the particulate's emission and the protein's absorption.31

Maximizing spectral overlap offers the potential to couple specific phosphors with appropriate biological conjugates, however sufficient energy needs to be supplied from the emitter that can elicit a response form the absorber. The sim-

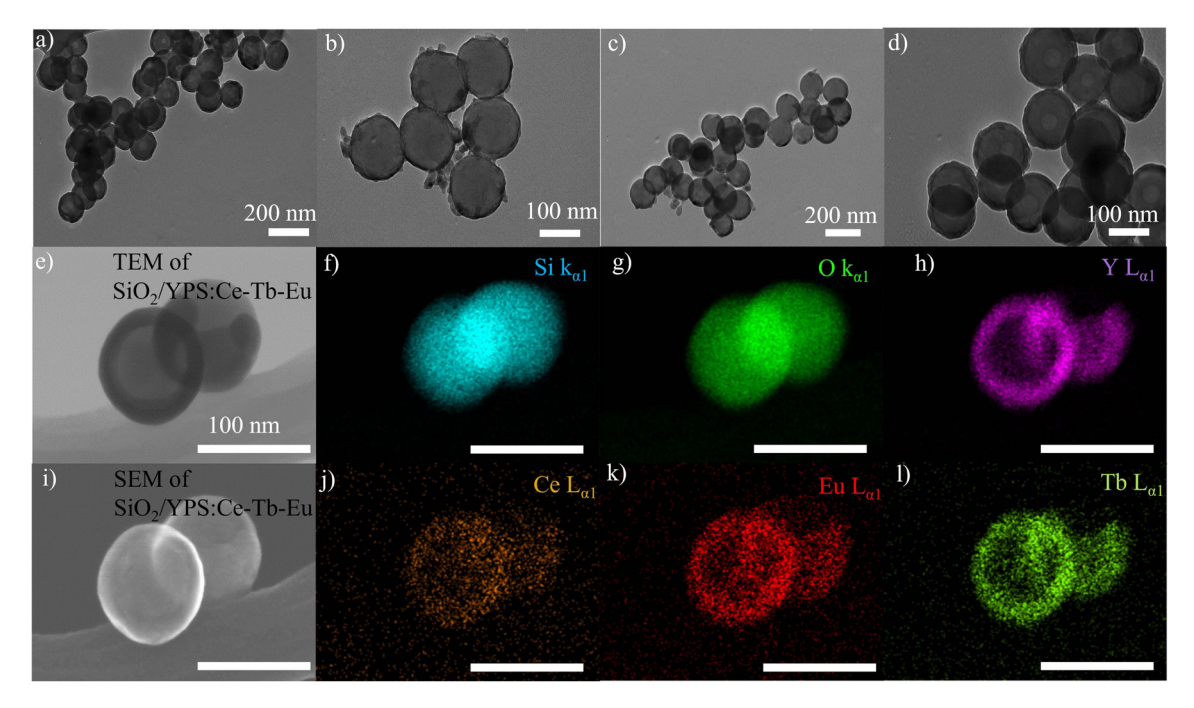


Fig. 2 Transmission electron microscopy (TEM) of (a) YPS:Ce, (b) YPS:Tb, (c) YPS:Eu, (d) YPS:Ce-Tb, and (e) YPS:Ce-Tb-Eu. EDS of YPS:Ce-Tb-Eu of (f) silicon, (g) oxygen, and (h) yttrium. (i) Scanning electron microscopy (SEM) of YPS:Ce-Tb-Eu. EDS of the rare earth emitters in YPS:Ce-Tb-Eu of (j) cerium, (k) europium, and (l) terbium.

Nanoscale Paper

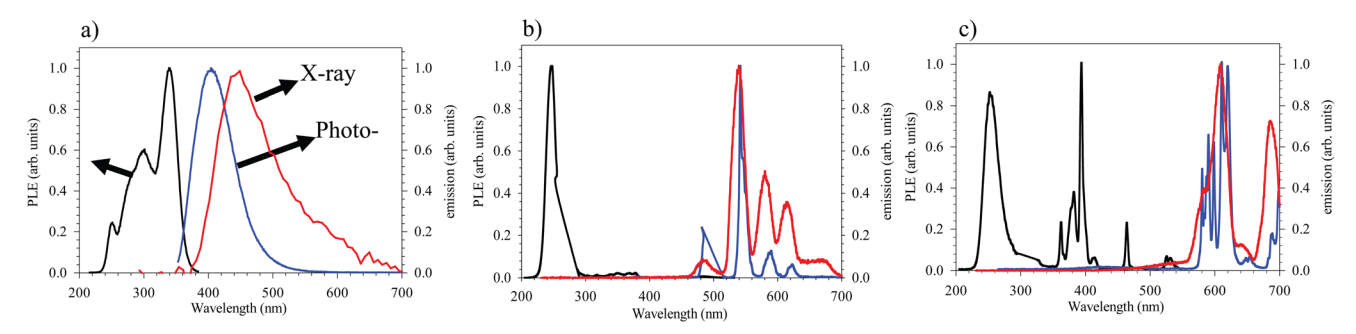


Fig. 3 Photoluminescence excitation (PLE), photoluminescence (PL), and radioluminescence (RL) of YPS mono-doped with (a) Ce³⁺, (b) Tb³⁺, and (c) Eu³⁺.

plest method to increase the light output of doped inorganic phosphors is by controlling the dopant concentration and by multi-doping the system. In this report three different concentrations of terbium and europium were investigated as a baseline to then optimize the multi-doped system that have been reported to enhance the photoluminescence of inorganic phosphors. Both photoluminescence (excited at 250 nm) and X-ray luminescence of YPS:Tb and YPS:Eu doped at different concentrations relative to yttrium were measured (Fig. 4). Terbium was doped at 1, 3 and, 10 mol% while europium was doped at 1, 10 and 15 mol%. No spectral shifts or luminescence quenching were observed throughout the study. For the mono-doped system of terbium, the integrated intensity of both radio- and photoluminescence (excited at 250 nm) increased linearly with doping concentration suggesting an overall increase in its optical light output. Not sur-

prisingly, terbium did not absorb the excitation energy at 338 nm which is the same excitation energy that is optimally absorbed by cerium. Europium on the other hand has multiple excitation bands between 250 nm-550 nm with an emission spectrum with noticeable integrated intensity when excited at both 338 nm and 250 nm. Interestingly, YPS:Eu doped at 10 mol% and 15 mol% showed no difference in its optical output in its photoluminescence when excited at 250 nm. However, the X-ray luminescence of the europium doped system increased its light output linearly with europium concentration. The results from YPS:Eu can be explained by the experimental setup in which, broadband bremsstrahlung X-rays were used and this high energy excitation source will excite the electrons from the valence band as well as the electrons in core band increasing the probability for exciton formation.

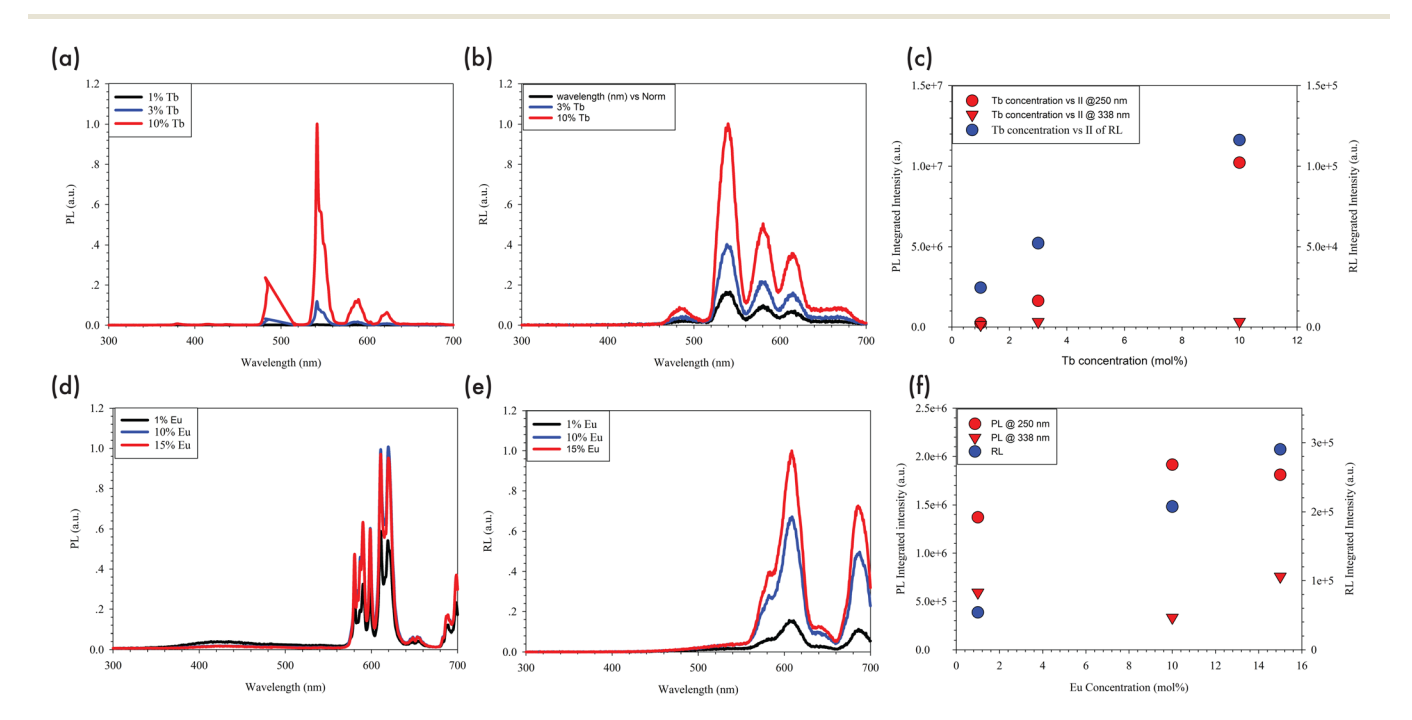


Fig. 4 (a) Photoluminescence (excited at 250 nm) and (b) radioluminescence of YPS:Tb when doped at 1, 3 and 10 mol% of terbium. (c) Optical output of YPS:Tb when excited by UV radiation at 250 nm, 338 nm, and X-rays, (d) Photoluminescence (excited at 250 nm) and (e) radioluminescence of YPS:Eu when doped at 1, 10 and 15 mol% of europium. (f) Optical output of YPS:Eu when excited by UV radiation at 250 nm, 338 nm, and X-rays.

Paper Nanoscale

The results from the mono-doped system provides a guide for multi-doped systems using cerium as a sensitizer for terbium. Initially the PL of mono-doped YPS:Tb (10 mol%) was compared to YPS:Ce-Tb (Fig. 5a). When excited at the Ce³⁺ optimal excitation wavelength (338 nm), the co-doped system has the emission profile of both Ce³⁺ and Tb³⁺ confirming energy transfer between the two dopants.32 Energy transfer efficiency from the sensitizer to the activator can be quantified through:33

$$\eta = 1 - \frac{I}{I_0}$$

where η is the energy transfer efficiency between the sensitizer and the activator, I is peak emission intensity of the sensitizer with the activator and I_0 is the peak emission intensity without the activator. In order to study energy transfer between Ce³⁺ and Tb³⁺, four concentrations of terbium were selected (1%, 3%, 5%, and 10% relative to yttrium) while cerium was kept at a constant concentration at 0.75% relative to yttrium. The η of the co-doped system was measured when excited at 250 nm and 338 nm, saturating at 90% and 65%, respectively (Fig. 5b). The Tb³⁺ emission dominates when the co-doped YPS particulates were excited by X-rays. The radioluminescence integrated intensity of the co-doped system exceeded the mono-doped Tb³⁺ series (Fig. 5c). This suggests that energy transfer is still occurring under X-ray excitation and enhances the overall light output of the nanoparticles. The highest total light output observed between the four samples was at a concentration of 0.75% cerium and 3% of terbium (Fig. 5d). The dominant energy transfer pathways can be suggested in Fig. 5e by the following: (1) electrons from Ce3+ ground state are excited to the 5d orbitals, (2) some of the Ce³⁺ electrons emit and relax to respective lower energy states, while some of the electrons transfer energy from the 5d states to the 5D3 state of Tb3+ through dipole-quadrupole interactions, (3) the excited electrons in the ⁵D₃ state nonradiatively decays to the ⁵D₄ state, which then relaxes to the ground state of Tb³⁺ giving a strong green emission.34

The presence of Tb³⁺ in a tri-doped system of Ce³⁺ and Eu³⁺ creates an ion-bridge where cerium acts as a sensitizer for terbium, which can then transfer energy to europium.³⁵ The photoluminescence of the cerium-europium co-doped system is compared to a cerium-terbium-europium tri-doped system (Fig. 6a). When excited at 338 nm the co-doped system only has a cerium photoluminescence band where the emission diminishes due to metal-metal charge transfer between cerium and europium ($Ce^{3+} + Eu^{3+} \rightarrow Ce^{4+} + Eu^{2+}$) where Ce^{4+} is non-radiative. When terbium is introduced the metal-metal charge transfer process is reduced by a cerium to terbium energy transfer, a phenomenon that was previously seen to effectively enhance the emission of terbium. In this event, terbium acts as a sensitizer for europium allowing some of the terbium excited state to leak into the europium ion. This results in a broadband emission that span the majority of the visible spectrum from 350 nm-700 nm from the initial 338 nm irradiation. Introducing a greater concentration of

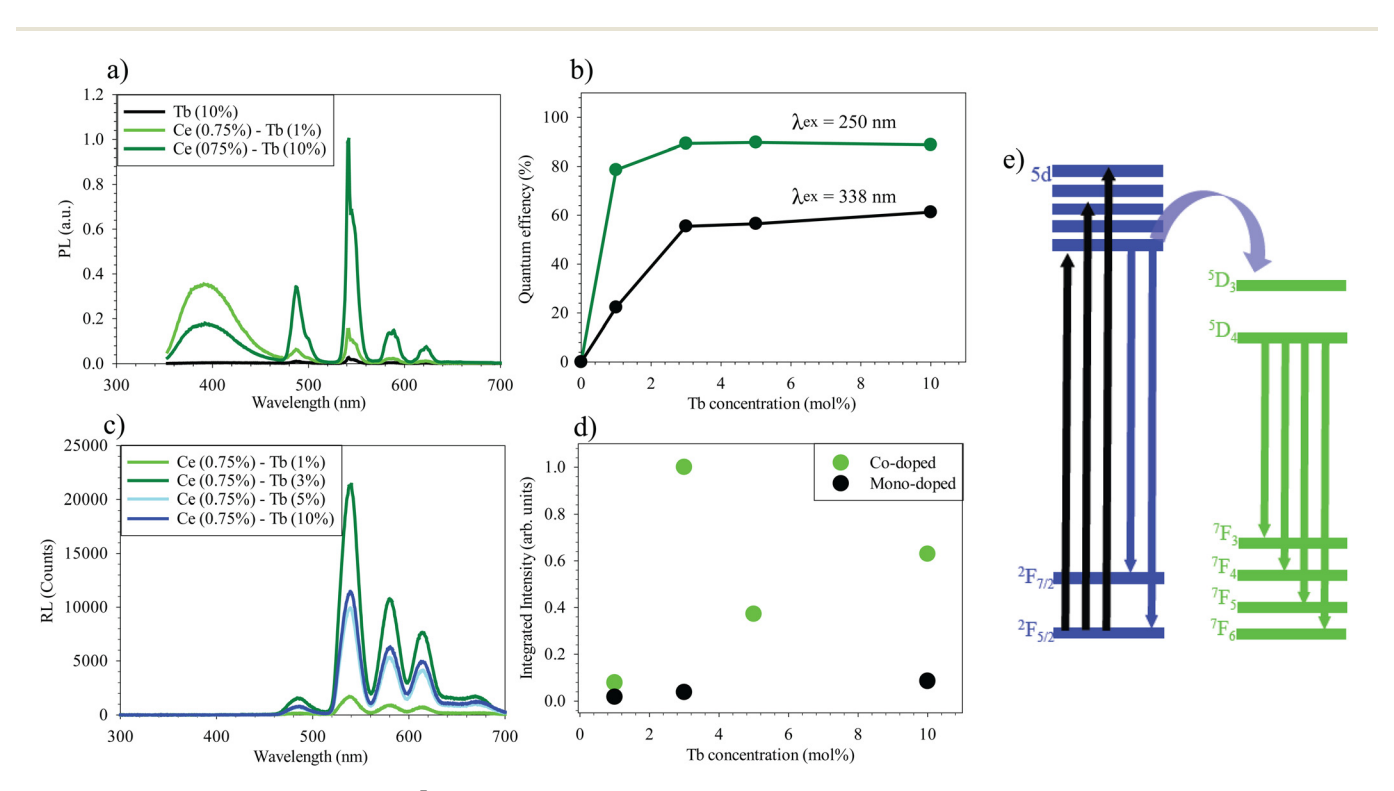


Fig. 5 (a) PL of YPS mono-doped with Tb³⁺ compared to a co-doped system. (b) Quantum efficiency of the co-doped system when excited at 338 nm and 250 nm. (c) RL of the co-doped system and its (d) integrated intensity when compared to mono-doped YPS:Tb. (e) Energy transfer from cerium to terbium.

a) b) 15000 15000 Ce(0.75%) - Tb (1%) - Eu(15%) Ce (0.75%) - Tb (0%) - Eu (15%) Ce(0.75%) - Tb (10%) - Eu(15%) Ce (0.75%) - Tb (10%) - Eu (15%) Ce(0.75%) - Tb (15%) - Eu(15%) Ce (0.75%) - Tb (15%) - Eu (15%) Photoluminescence (c.p.s) 12000 10000 RL (counts) 9000 6000 5000 3000 400 500 600 700 300 400 500 600 700 Wavelength (nm) Wavelength (nm) d) c) 1e+6 Tri-doped system Mono-doped system RL integrated intensity (a.u.) 8e+5 6e+5 $2e \pm 5$

Nanoscale

Fig. 6 (a) PL of YPS tri-doped with Ce³⁺, Tb³⁺, and Eu³⁺. (b) RL of the tri-doped YPS series and its respective (c) integrated intensity values compared to the brightest mono-doped YPS:Eu (15%). (d) Energy transfer scheme from cerium to terbium to europium.

15

12

Tb concentration relative to Y (mol%)

terbium reduces the ion-ion distances, allowing terbium ions to cross relax with one another and making it more efficient to transfer its energy to europium as suggest by the decrease in the cerium and terbium bands and a increase in the europium bands. Under X-ray excitation the tri-doped system showed a slight emission at 550 nm, which is where terbium can emit, along with two dominant europium bands at 600 nm and 680 nm (Fig. 6b). When the RL integrated intensity of YPS:Ce-Tb-Eu was compared to YPS:Eu at 15 mol%, an initial decrease in output was observed with a 1 mol% of terbium, followed by an overall increase in its optical output at 10 mol% and 15 mol% (Fig. 6a). The RL optical output is three times greater than the YPS:Eu 15 mol% mono-doped system, which suggests that the terbium bridge transfers energy from cerium and terbium to europium. The four possible interactions to explain the photoluminescence are: (1) cerium absorbs the UV irradiation and generates emission, (2) excited state cerium transfers energy to terbium and causes a green emission, (3) a terbium ion is in close proximity with a neighboring terbium ion and cross relaxes to emit or transfer to europium which would emit a photon corresponding to europium's emission,

3

and (4) europium absorbs the incoming irradiation and emits. The resulting spectrum would be a broad emission with characteristics of cerium, terbium and europium. When compared to the RL of YPS:Ce-Tb-Eu however, the dominant bands are from europium with only a negligible band from terbium and no cerium emission observed. This would suggest that the X-ray excitation source is assisting with the energy transfer process to become more efficient. This also implies that the use of opsins that are optimized for europium emission absorption would be the more efficient biological and optogenetic performers.

In this work a series of mono- and multi-doped (Ce³⁺, Tb³⁺, and Eu³⁺) YPS nanoparticles were synthesized by the HTMcR process. In the co-doped series, cerium and terbium energy transfer was observed by PLE/PL. Cerium was used as a sensitizer for terbium, which enhances the X-ray luminescence of terbium emission bands. In the tri-doped series, all three dopant bands were observed when excited at 338 nm. The PL traces implies that cerium acted as a sensitizer for terbium which allows terbium to act as a bridge for europium. By increasing the concentration of terbium, the ion-ion distance

Paper Nanoscale

between terbium is reduced and acted as a migrating pathway for europium to absorb energy from cerium and terbium. Using simple doping strategies, both the co- and tri-doped series exhibited enhancement in X-ray luminescence compared to their mono-doped counterpart. Both the multi-doped system exhibits promising X-ray luminescent properties that when coupled with the HTMcR can be applied to the biomedical field such as X-ray induced optogenetics and X-ray photodynamic therapy.

Materials and methods

All reagents were purchased from Alfa Aesar, Sigma Aldrich, and Acros Organics. Tetraethyl orthosilicate (TEOS) and 3-(trimethoxysilyl)propyl methacrylate (MPS) were purified by distillation under vacuum. Divinyl benzene (DVB) was purified by passing through a basic alumina oxide filter to remove the inhibitor. Azobisisobutyronitrile (AIBN) was recrystallized from methanol. All other reagents were used without additional purification.

Synthesis of YPS

Silica particles were synthesized by a modified Stöber process with TEOS (67.18 mmol, 15.0 mL) dissolved in ethanol (150 mL), followed by addition of water (15.0 mL) and NH₄OH (29.38% v/v, 5.0 mL). The reaction was stirred vigorously for 48 h and purified with water and centrifugation. The silica nanoparticles were dispersed in water (200 mL) for future experimental steps. Aliquots of the silica solution (2.5 mmol, 150 mg) were dispersed in 75 mL of water followed by dissolving selected amounts of rare earth (Y3+, Ce3+, Tb3+, Eu3+) nitrate hexahydrates (total of 0.75 mmol). Sodium bicarboante (2.51 mmol, 211 mg) was dissolved in 60 mL of water and titrated into to reaction vessel and stirred for 1 h. The HTMcR process was scaled to accommodate 125 mg of the core-shell particulates as previously reported. 12 The various doped YPS/ pDVB particulates were annealed at 1100 °C for 18 h under nitrogen environment followed by combustion at 800 °C for 1 h.

Material characterization

A Hitachi 9000 STEM was used to acquire TEM and EDS maps of the particulates, all samples were dispersed in methanol and drop casted onto a Formvar/Carbon 200 mesh TEM grid. RL of the particulates were excited by a Amptek Mini-X tungsten source at 25 kV and 158 μA and obtained by a DMI 5000M microscope, coupled to a DNS 300 spectrometer with a 150 lines per mm grating blazed at 500 nm, and with a cooled iDUS420BV CCD camera. Samples were packed in a 6.5 mm x 1.5 mm round flat washer on a quartz slide. UV luminescence measurements were taken on a Jobin Yvon Fluorolog 3-222 spectrometer. The powder X-ray diffraction (pXRD) measure-

ments were carried out on a Rigaku Ultima IV diffractometer using $Cu_{K\alpha}$ radiation ($\lambda = 1.5406$ Å). The powder diffraction data was recorded in 0.02° increments over a 2θ range of 5° to 65° at a scan speed of 1° min⁻¹. Experimental pXRD patterns were compared to single crystal structures reported in the

Conflicts of interest

There are no conflicts of interest to declare.

Acknowledgements

This material is based upon work supported by the National Science Foundation under Grant No. OIA-1632881.

References

- 1 C. Liu, Y. Hou and M. Gao, Are rare-earth nanoparticles suitable for in vivo applications?, Adv. Mater., 2014, 26(40), 6922-6932.
- 2 D. Kim, K. Shin, S. G. Kwon and T. Hyeon, Synthesis and biomedical applications of multifunctional nanoparticles, Adv. Mater., 2018, 30(49), e1802309.
- 3 G. Chen, H. Qiu, P. N. Prasad and X. Chen, Upconversion nanoparticles: Design, nanochemistry, and applications in theranostics, Chem. Rev., 2014, 114(10), 5161-5214.
- 4 T. Guo, Y. Lin, W. J. Zhang, J. S. Hong, R. H. Lin, X. P. Wu, J. Li, C. H. Lu and H. H. Yang, High-efficiency X-ray luminescence in eu(3+)-activated tungstate nanoprobes for optical imaging through energy transfer sensitization, Nanoscale, 2018, 10(4), 1607-1612.
- 5 W. Fan, P. Huang and X. Chen, Overcoming the achilles' heel of photodynamic therapy, Chem. Soc. Rev., 2016, 45(23), 6488-6519.
- 6 T. Matsubara, T. Yanagida, N. Kawaguchi, T. Nakano, J. Yoshimoto, S. P. Tsunoda, S.-ichiro Horigane, S. Ueda, S. Takemoto-Kimura, H. Kandori, A. Yamanaka and T. Yamashita, Remote control of neural function by x-rayinduced scintillation, Nat. Commun., 2021, 12, 1-12.
- 7 S. E. Derenzo, M. J. Weber, E. Bourret-Courchesne and M. K. Klintenberg, The quest for the ideal inorganic scintillator, Nucl. Instrum. Methods Phys. Res., Sect. A, 2003, 505(1-2), 111-117.
- 8 B. Cline, I. Delahunty and J. Xie, Nanoparticles to mediate X-ray-induced photodynamic therapy and cherenkov radiation photodynamic therapy, Wiley Interdiscip. Rev.: Nanomed. Nanobiotechnol., 2019, 11(2), e1541.
- 9 M. K. Burdette, Y. P. Bandera, E. Zhang, A. Trofimov, A. Dickey, I. Foulger, J. W. Kolis, K. E. Cannon, A. F. Bartley, L. E. Dobrunz, M. S. Bolding, L. McMahon and S. H. Foulger, Organic fluorophore coated polycrystalline ceramic lso:ce scintillators for x-ray bioimaging, Langmuir, 2019, 35(1), 171–182.

10 W. Sun, Z. Zhou, G. Pratx, X. Chen and H. Chen, Nanoscintillator-mediated x-ray induced photodynamic

therapy for deep-seated tumors: From concept to biomedical applications, Theranostics, 2020, 10(3), 1296-1318.

Nanoscale

- 11 A. F. Bartley, K. Abiraman, L. T. Stewart, M. I. Hossain, D. M. Gahan, A. V. Kamath, M. K. Burdette, S. Andrabe, S. H. Foulger, L. L. McMahon and L. E. Dobrunz, Lso:ce inorganic scintillators are biocompatible with neuronal and circuit function, Front. Synaptic Neurosci., 2019, 11, 24.
- 12 E. Zhang, Y. P. Bandera, A. Dickey, I. Foulger, J. W. Kolis and S. H. Foulger, Development of dispersible radioluminescent silicate nanoparticles through a sacrificial layer approach, J. Colloid Interface Sci., 2020, 1128-1135.
- 13 J. C. G. Bunzli, S. Comby, A. S. Chauvin and C. D. B. Vandevyver, New opportunities for lanthanide luminescence, J. Rare Earths, 2007, 25(3), 257-274.
- 14 J.-C. G. Bunzli, Lanthanide luminescence for biomedical analyses and imaging, Chem. Rev., 2010, 110, 2729-2755.
- 15 Y. Ning, M. Zhu and J.-L. Zhang, Near-infrared (nir) lanthanide molecular probes for bioimaging and biosensing, Coord. Chem. Rev., 2019, 399, 213028.
- 16 S. I. Weissman, Intramolecular energy transfer the fluorescence of complexes of europium, J. Chem. Phys., 1942, **10**(4), 214-217.
- 17 K. Meyssamy, K. Riwotzki, A. Kornowski, S. Naused and M. Haase, Wet-chemical synthesis of doped colloidal nanomaterials: Particles and fibers of lapo4:eu, lapo4:ce, and lapo4:ce,tb, Adv. Mater., 1999, 11(10), 840-844.
- 18 W. Xia, Y. Zhang, J. Xiong, S. Hu, J. Yu, Y. Zhang, Y. Wan and J. Yang, Facile synthesis, morphology and tunable photoluminescence properties of bamgf4:ce3+/tb3+/eu3+ phosphors, CrystEngComm, 2019, 21(2), 339-347.
- 19 X. Qin, J. Xu, Y. Wu and X. Liu, Energy-transfer editing in lanthanide-activated upconversion nanocrystals: A toolbox for emerging applications, ACS Cent. Sci., 2019, 5(1), 29-42.
- 20 T. Yanagida, Study of rare-earth-doped scintillators, Opt. Mater., 2013, 35(11), 1987-1992.
- 21 W. Zhang, X. Zhang, Y. Shen, F. Shi, C. Song, T. Liu, P. Gao, B. Lan, M. Liu, S. Wang, L. Fan and H. Lu, Ultra-high fret efficiency nagdf4: Tb(3+)-rose bengal biocompatible nanocomposite for x-ray excited photodynamic therapy application, Biomaterials, 2018, 184, 31-40.
- 22 R. Berry, M. Getzin, L. Gjesteby and Ge Wang, X-optogenetics and u-optogenetics: Feasibility and possibilities, Photonics, 2015, 2(1), 23-39.
- 23 Q. Chen, J. Wu, X. Ou, B. Huang, J. Almutlaq, A. A. Zhumekenov, X. Guan, S. Han, L. Liang and Z. Yi, All-

- inorganic perovskite nanocrystal scintillators, Nature, 2018, **561**(7721), 88-93.
- 24 M. J. Weber, Inorganic scintillators: today and tomorrow, J. Lumin., 2002, 100(1-4), 35-45.
- 25 X. Zhao, S. He and M. C. Tan, Design of infraredemitting rare earth doped nanoparticles and nanostructured composites, J. Mater. Chem. C, 2016, 4(36), 8349-8372.
- 26 Z. Sun, M. Li and Y. Zhou, Recent progress on synthesis, multi-scale structure, and properties of v-si-o oxides, Int. Mater. Rev., 2014, 59(7), 357-383.
- 27 S. V. Eliseeva and J. C. Bunzli, Lanthanide luminescence for functional materials and bio-sciences, Chem. Soc. Rev., 2010, 39(1), 189-227.
- 28 F. Zhang, J. Li, J. Shan, L. Xu and D. Zhao, Shape, size, and phase-controlled rare-earth fluoride nanocrystals with optical up-conversion properties, Chem. - Eur. J., 2009, **15**(41), 11010-11019.
- 29 P. C. Ricci, C. M. Carbonaro, R. Corpino, C. Cannas and M. Salis, Optical and structural characterization of terbium-doped y2sio5phosphor particles, J. Phys. Chem. C, 2011, 115(33), 16630-16636.
- 30 M. D. Dramićanin, B. Viana, Ž. Andrić, V. Djoković and A. S. Luyt, Synthesis of y2sio5:eu3+ nanoparticles from a hydrothermally prepared silica sol, J. Alloys Compd., 2008, 464(1-2), 357-360.
- 31 L. Fenno, O. Yizhar and K. Deisseroth., The Development and Application of Optogenetics, volume 34 of Annual Review of Neuroscience, Annual Reviews, Palo Alto, 2011, pp. 389-412.
- 32 D. Chiriu, L. Stagi, C. M. Carbonaro, R. Corpino and P. C. Ricci, Energy transfer mechanism between ce and tb ions in sol-gel synthesized yso crystals, Mater. Chem. Phys., 2016, 171, 201-207.
- 33 X. Zhang, L. Zhou, Qi Pang, J. Shi and M. Gong, Tunable luminescence and ce3+ \rightarrow tb3+ \rightarrow eu3+ energy transfer of broadband-excited and narrow line red emitting y2sio5: ce3+, tb3+, eu3+phosphor, J. Phys. Chem. C, 2014, 118(14), 7591-7598.
- 34 P. Ghosh, A. Kar and A. Patra, Energy transfer study between ce3+ and tb3+ ions in doped and core-shell sodium yttrium flouride nanocrystals, Nanoscale, 2010, 2(7), 1057.
- 35 J. Zhou and X. Zhiguo, Luminescence color tuning of ce3+, tb3+ and eu3+ codoped and tri-doped bay2si3o10 phosphors via energy transfer, J. Mater. Chem. C, 2015, 3, 7552-7560.